Journal of Materials Chemistry A

Accepted Manuscript

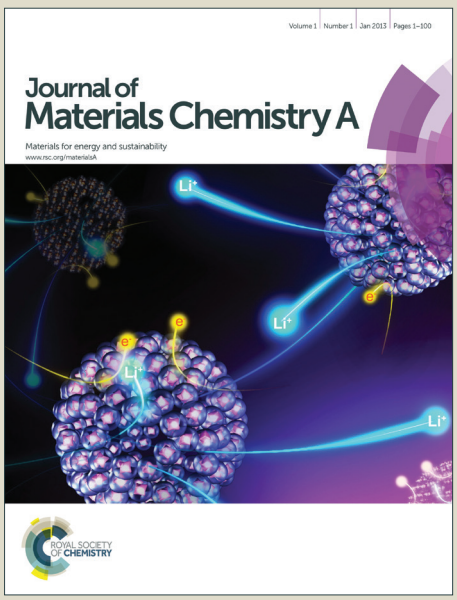

ROYAL SOCIETY OF CHEMISTRY

www.rsc.org/materialsA

Revised manuscript submitted to *J. Mater. Chem. A*

Ultrastable iridium-ceria nanopowders synthesized in one step by solution combustion for catalytic hydrogen production

Thanh-Son Nguyen, Georgeta Postole, Stéphane Loridant, Françoise Bosselet, Laurence Burel, Mimoun Aouine, Laurence Massin, Patrick Gélin, Franck Morfin, and Laurent Piccolo*

Institut de recherches sur la catalyse et l'environnement de Lyon (IRCELYON), UMR 5256 CNRS & Université Lyon 1, 2 avenue Albert Einstein, F-69626 Villeurbanne, France

Abstract

Mesoporous ceria loaded with 0.06-0.93 wt% iridium was synthesized in one step by the ambient air combustion of an aqueous solution of ceric ammonium nitrate, ammonium hexachloroiridate, and glycine fuel. The structural properties of the powders, and the influence of such parameters as Ir loading and thermochemical post-treatments, were investigated combining aberration-corrected HRTEM, SEM, *in situ* XRD, XPS, DRIFTS, and Raman spectroscopy. The materials, which appeared spongy at the micrometer scale, exhibited *ca.* 30 nm-sized ceria crystallites with a layered structure at the nanoscale. After reducing treatments, Ir nanoparticles anchored at the surface of ceria grains were identified, and their size (*ca.* 2 nm) did not evolve upon further heating at up to 900 °C. A detailed picture of the Ir-CeO_2 interface could be established, with the presence of Ir^{x+}-O^{2-}-Ce^{3+} entities along with oxygen vacancies. The powders loaded with only 0.1 wt% Ir were successfully employed as catalysts for the production of hydrogen from methane and water in low-steam conditions at 750 °C. Due to their higher Ir dispersion and stronger Ir-CeO_2 interaction, the combustion-synthesized materials outperformed their conventionally prepared counterparts in terms of activity and stability, making them promising as active catalytic layers for solid-oxide fuel cells integrating the gradual internal reforming concept.

* Corresponding author. E-mail: laurent.piccolo@ircelyon.univ-lyon1.fr

Revised manuscript submitted to *J. Mater. Chem. A*

Introduction

Due to the unique redox properties of ceria, ceria-based materials are of paramount importance for heterogeneous catalysis.[1–3] Ceria-supported noble metals (typically Pt/CeO_2) are commonly used as automotive three-way catalysts to simultaneously reduce nitric oxides, and oxidize carbon monoxide and unburnt hydrocarbons. In this application, the CeO_2 support operates as an oxygen buffer by releasing oxygen under reducing conditions and storing oxygen under oxidizing conditions. Other applications of ceria-noble metal catalysts include oxidation of volatile organic compounds, diesel soot combustion, synthesis of high-value chemicals from biomass, hydrogen production from steam reforming and water-gas shift, and hydrogen purification from the preferential oxidation of CO.[1,4]

Due to its high ionic and electronic conductivities above 600 °C, Gd-doped CeO_2 has become attractive for solid oxide fuel cells (SOFCs), although Y_2O_3-stabilized ZrO_2 (YSZ) and Ni/YSZ are currently more popular as electrolyte and anode catalyst materials, respectively.[5,6] The role of the anode catalyst is to use the oxygen ions that diffuse through the electrolyte to electrochemically oxidize the hydrogen fuel, producing electricity, heat, and water. If the SOFC is fed with a light hydrocarbon such as methane, the anode should also include a catalytic function for internal steam methane reforming (SRM, $CH_4 + H_2O \rightarrow CO + 3H_2$).[7] The principle of the so-called "gradual internal reforming" (GIR) is that SRM and electrochemical oxidation of hydrogen can be self-sustained, since the latter reaction produces the water needed by the former one.[8] The main advantages of GIR are a delocalization of the high endothermicity of steam reforming, and a potential operation in dry methane after initiation of the reforming reaction with a small amount of steam. As the use of GIR requires the development of specific catalysts moderately active in steam reforming but highly resistant to carbon deposition and sulfur poisoning, the efficiency of noble metal-based catalysts with low metal loading (dopant level) can minimize the cost, making them versatile for this application. In this context, recent findings suggest that a CeO_2 layer loaded with small amounts of iridium could be an efficient SRM catalyst protecting the Ni-based anode, due to its high resistance to poisoning.[9–13] Indeed, both CH_4 and CO decompose on Ni, leading to coke formation. Moreover, in the case of methane-based fuels (natural gas, biogas), the catalyst must be resistant to sulfur-containing compounds.

Combustion synthesis forms a class of relatively simple and inexpensive methods for preparing advanced solid materials, generally (mixed) metal oxides. It relies on the fact that an exothermic reaction can be self-sustained by the heat it generates, *i.e.* without external energy supply, except for ignition. Depending on the solid, liquid, or gaseous nature of the metal precursor phase, the method is called self-propagating high-temperature synthesis (SHS), solution combustion synthesis (SCS), or

Revised manuscript submitted to *J. Mater. Chem. A*

flame synthesis, respectively. SCS consists in the fast and self-sustained combustion of a pre-heated aqueous solution of metallic salt (usually nitrate) and an organic fuel (*e.g.* urea, oxalyl dihydrazide, or glycine). The solid oxide material obtained is generally nanocrystalline, making it suitable to heterogeneous catalysis, in particular for high-temperature processes like hydrocarbon reforming reactions, which require highly stable catalysts.[14–20]

The synthesis of oxides loaded with precious metals by combustion is much less conventional. Hegde and coworkers used the SCS method to prepare, in a single step, solid oxides mostly based on CeO_2 and TiO_2 loaded with noble metals.[21,22] Using XRD, XPS and EXAFS, the authors reported the formation of so-called $Ce_{1-x}M_xO_{2-\delta}$ solid solutions (herein referred to as M-CeO_2) with M being Cu, Pd, Pt, or Rh.[23–26] According to the authors, the atomic dispersion of the metals, a large fraction of which would be substituted in the ceria lattice as cations, gives rise to an exceptionally high catalytic activity in such reactions as CO oxidation and NO reduction. SCS was also employed by other groups to prepare noble metal nanoparticles supported on *e.g.* ceria or ceria-zirconia for catalyzing various reactions, including steam reforming.[27–35] Noticeably, from HRTEM observations of Pd-CeO_2 and DFT calculations, Colussi *et al.* identified stable ordered Pd-O-Ce superstructures suggested to be responsible for superior catalytic performances in methane combustion.[31,33] Unlike Pt-group metals combined with ceria, Au/CeO_2 synthesized in one step with the SCS method (using urea fuel) does not exhibit a high metal dispersion (5-25 nm particles).[28]

To the best of our knowledge, the synthesis of Ir-based materials by SCS was never reported to date. Moreover, studies of the influence of thermal/chemical post-treatments on the material structure are lacking, although such treatments are of key importance for the so-called activation of the catalyst.[32] In this article, we highlight the applied interest of the Ir-CeO_2 material by briefly showing its excellent catalytic SRM performances. Then, we present a comprehensive structural investigation of the combustion-synthesized powders, both as-prepared and submitted to several treatments. To this aim, we made extensive use of state-of-the-art microscopic and spectroscopic techniques, leading to a detailed description of the metal-oxide interface.

Experimental Section

Synthesis. A series of CeO_2 and Ir-CeO_2 powders (see Table 1) was prepared by solution combustion synthesis (SCS), using ceric ammonium nitrate, *i.e.*, CAN [$(NH_4)_2Ce(NO_3)_6$, Sigma-Aldrich, 99.99%], serving both as ceria precursor salt and oxidizing agent. Ammonium hexachloroiridate (IV)

$[(NH_4)_2IrCl_6$, Strem Chemicals, 99%] was employed as Ir precursor salt. Glycine ($C_2H_5NO_2$, Sigma-Aldrich, 99%) was used as fuel. Oxalyl dihydrazide (ODH, $C_2H_6N_4O_2$) fuel was also tried but gave unsatisfactory results. The CAN:glycine:Ir precursor mixture composition was chosen to obtain stoichiometric proportions of oxidizer and fuel (*i.e.*, with the oxidizing/reducing valence ratio of the redox mixture equal to 1) [36] and to reach the desired Ir loading (from 0.1 to 1 wt%).

Practically, a borosilicate beaker (300 cm^3) containing a mixture of CAN (5.00 g), glycine (1.82 g), $(NH_4)_2IrCl_6$ if needed (4-42 mg for 0.1-1 wt% Ir-CeO_2), and 30 mL deionized water was introduced into a muffle furnace (Carbolite ELF 11/6) maintained at 350 °C. At the point of complete dehydration (5-10 min), the solution started boiling and foaming, and ignition took place after a few seconds with rapid evolution of a large quantity of gases. This yielded a voluminous solid product within a few minutes. The powder color ranged from pale yellow to grey, going from pure CeO_2 to 1 wt% Ir-CeO_2.

Depending on the targeted catalytic reaction, a post-synthesis treatment can be needed to activate the catalysts by *e.g.* generating metallic nanoparticles (see below). A standard treatment of the Ir-CeO_2 samples consisted in heating them at 400 °C in H_2 flow in order to reduce the metal and remove residual carbon impurities issuing from the SCS. Alternatively, in some cases the samples were submitted to an oxidizing-reducing treatment (so-called "oxred"), which proved to be even more efficient than the standard pretreatment in terms of catalytic methane reforming activity.[37] It consisted in heating the sample at 300 °C in 12% O_2 + Ar flow before heating it at 500 °C in 12% H_2 + Ar flow. The pre-oxidation allowed burning the carbonaceous residues present in the freshly-prepared samples. In all cases, the heating ramp was 5 °C min^{-1}, the heating plateau lasted 2 h, and the gas flow rate was 7 L h^{-1}.

In addition, three catalysts were prepared by conventional incipient wetness impregnation (IWI) of SCS ceria in order to compare their structure, stability and catalytic performances with those of the SCS samples. $(NH_4)_2IrCl_6$ or $Ir(C_5H_7O_2)_3$ (iridium tris(acetylacetonate), Sigma-Aldrich, 97%) were used as metal precursors. After impregnation of ceria (up to pore filling) with Ir chloride dissolved in water or $Ir(acac)_3$ dissolved in toluene, the samples were allowed to maturate in ambient conditions for 2 h and were dried at 120 °C overnight. Then, the Ir chloride/ceria samples were calcined in air flow at 500 °C for 2 h, and afterwards reduced in H_2 flow at 400 °C for 3 h. The $Ir(acac)_3$/ceria sample was directly reduced in H_2 flow at 500 °C for 6 h. In all cases, the heating ramp was 5 °C min^{-1} and the gas flow rate was 7 L h^{-1}.

Characterization. The samples were characterized by elemental analysis, N_2 adsorption volumetry, thermogravimetric measurements (TG-DTA-MS), X-ray diffraction (XRD, standard and *in situ* experiments), scanning electron microscopy (SEM), aberration-corrected high-resolution transmission electron microscopy (HRTEM), X-ray photoelectron spectroscopy (XPS) combined with a pretreatment cell, and infrared spectroscopy of adsorbed CO (CO-DRIFTS). The details of the apparatus and procedures are available in ESI.

Catalytic tests and temperature-programmed experiments. Catalytic activity experiments were carried out at 750 °C in a continuous flow system at atmospheric pressure, using a tubular U-shaped quartz reactor (internal diameters of 15 and 4 mm for 100 mg CeO_2 and 10 mg Ir-CeO_2, respectively). For steam reforming of methane, the reactant mixture consisted of 50 vol% CH_4 and 5 vol% H_2O in N_2 at a total flow rate of 7 L_{NTP} h^{-1}. Prior to the catalytic tests, the samples were pre-conditioned at 900 °C in N_2 flow for 2 h. The gas flows were regulated by pre-calibrated mass flow controllers. Suitable water vapor concentration in the reaction mixture was obtained by flowing the adequate mixture of CH_4 and N_2 dry gases throughout a saturator containing distilled water and maintained at 33.1 °C. An M&C ECP gas cooler maintained at 3 °C was used to reduce the steam concentration in the feed in order to allow for a reliable analysis by gas chromatography. CH_4, H_2, CO and CO_2 were analyzed with a Varian micro-GC equipped with appropriate columns (molecular sieve 5Å and Porapak Q) and thermal conductivity detectors (TCD). CH_4 (N5.5 purity) and N_2 (N5.0 purity) gases were supplied by Linde.

Temperature-programmed reduction (TPR) was performed under diluted dry methane (3 mol% CH_4 in N_2). Before performing CH_4-TPR, the fresh samples were pretreated under nitrogen flow (7 L_{NTP} h^{-1}) at 900 °C for 2 h. Then they were cooled down to RT, and afterwards heated at 5 °C min^{-1} to 900 °C in the reactive gas mixture. For temperature-programmed oxidation (TPO), a mixture of 3 mol% O_2 in N_2 flow (7 L_{NTP} h^{-1}) was applied, and the samples were heated at 5 °C min^{-1} from RT to 900 °C. For the TPO experiments performed after the SRM tests, the reactor was previously purged with nitrogen and cooled down to RT in the same atmosphere. The bench used for the TP experiments was the same as for catalytic testing.

3. Results and discussion

A series of Ir-CeO_2 samples with various Ir loadings (from 0 to 1 wt%) was prepared by solution combustion synthesis (SCS). Their structure and catalytic performances were extensively investigated

and correlated with several thermochemical pretreatments. Table 1 summarizes the general characteristics (Ir content, ceria crystallite size, lattice parameter, and surface area) of the as-prepared ("fresh") CeO_2 and Ir-CeO_2 samples. The results for commercial ceria (Grace) and three catalysts prepared by incipient wetness impregnation (IWI) of combustion-synthesized ceria with Ir precursors are also reported in Table 1 for comparison. As determined from N_2 adsorption volumetry, following the standard glycine-nitrate SCS process, BET specific surface areas vary in the range 10-55 m^2/g. The N_2 physisorption isotherms (Fig. S1, ESI) are intermediates between types II and type IV, indicating the presence of mesopores with a broad size distribution that continues into the macropore domain.[38]

Catalytic performances. The combustion-synthesized materials with low metal loadings (0.1-0.3 wt% Ir) were evaluated as catalysts in the steam reforming of methane at 750 °C (a detailed catalytic study will be reported elsewhere[37]). Ir-CeO_2 prepared by SCS and submitted to the aforementioned "ox-red" pretreatment was compared to pristine ceria (itself prepared by SCS) and to a catalyst prepared by conventional IWI of the same ceria with Ir. Note that the same Ir precursor ($(NH_4)_2IrCl_6$) was used in both one-step SCS and SCS+IWI cases, and that the "ox-red" treatment was inherent to our IWI method.

Figure 1a displays the methane consumption rates versus time-on-stream, along with the product distributions (inset). Quantitative data are also reported in Table S1. It appears that the reaction rate is greatly increased by the addition of 0.1 wt% Ir to CeO_2, as previously shown for impregnation catalysts.[13] Iridium is thought to facilitate the rate-determining step, namely methane dissociation. The reducibility of ceria allows for fast diffusion of surface oxygen[2,39] and its reaction with CH_x species to form CO and H_2, in spite of the H_2O-poor conditions used here. As shown in inset, the formed products are H_2 (75-76 %), CO (21-23 %), and CO_2 (1-3 %) on both Ir-containing catalysts, whereas CO_2 is favored over CO on pure ceria.[37]

Figure 1a reveals that with the SCS catalyst, a similar activity is obtained while using three times less iridium than with an IWI catalyst, i.e., the rate per Ir weight is about three times higher for the SCS catalysts than for the IWI ones. Two additional 0.1 wt% Ir-CeO_2 samples (samples B and D in Table 1) were synthesized the same way and showed similar SRM performances, which proves the reproducibility of the preparation method. Note that a 0.1 wt% Ir IWI catalyst, prepared by (Cl-free) acetylacetonate impregnation and direct reduction, was also investigated for comparison, and equally showed lower activity per metal weight with respect to the SCS catalyst.[37]

Revised manuscript submitted to *J. Mater. Chem. A*

Furthermore, the IWI sample is seen to deactivate continuously, whereas the SCS sample exhibits slight activation after *ca.* 7 h on stream. A long-term catalytic test shows that Ir-CeO_2 loses only 10 % of its activity after 3 days on stream (Fig. S2).

The amount of carbon deposited on the surface of the samples during the reaction was investigated by post-reaction temperature-programmed oxidation (TPO). Fig. S3 shows that CO_2 desorbs at lower temperature from Ir-CeO_2 than from Ir-CeO_2 (IWI). This can be ascribed to the weaker interaction of deposited carbon with Ir in the SCS catalyst. This aspect may favor the SCS catalyst in terms of activity and stability. However, one should be aware that the amount of deposited C (see Fig. S3) is extremely low if one compares with conventional Ni catalysts.

Reactivity toward methane. Temperature-programmed reduction experiments using methane (TPR-CH_4) were performed to get insight into the reactivity of CH_4 with CeO_2 and Ir-CeO_2-oxred materials. The TPR profiles of Fig. 1b were obtained after an activation step in inert atmosphere at 900 °C (as before SRM tests).

Methane starts to react with pure CeO_2 at *ca*. 600 °C by producing traces amounts of CO_2 (not shown in Fig. 1b, see Fig. S4). CO is formed from *ca*. 630 °C, and its yields increases continuously up to 900 °C. The formation of CO/CO_2 is due to the reaction between CH_4 and reducible oxygen species of the ceria lattice, which implies the reduction of a certain amount of Ce^{4+} into Ce^{3+} during the TPR experiment.[37]

On the Ir-containing samples, CH_4 starts to be converted into CO/H_2 at 375 °C (SCS) and 390 °C (IWI). These temperatures are much lower than for CeO_2, indicating that the addition of iridium to ceria catalyzes both the dissociative adsorption of CH_4 and the reduction of ceria. Ir-CeO_2 shows a main reduction peak centered at *ca*. 570 °C, while in the case of Ir/CeO_2 (IWI) this peak is centered at *ca*. 650 °C. This suggests a higher reactivity of the SCS material toward methane, with respect to the IWI sample. This directly correlates with the higher SRM activity of the SCS catalyst (Fig. 1a). The gradual decrease of the CO formation rate at *ca*. 800 °C (Fig. 1b) indicates a shortage of the oxygen supplied by the ceria lattice. From C mass balance calculations, carbonaceous deposits could be formed together with H_2 around this temperature, although in limited amounts (0.5 wt% C for Ir-CeO_2 and 0.8 wt% C for Ir/CeO2 (IWI), as found by TPO performed after the TPR, see Fig. S5).

With the objective of identifying the factors controlling the efficiency of the combustion-synthesized catalysts, the bulk and surface structures of CeO_2 and Ir-CeO_2 materials, fresh and submitted to

several treatments, were investigated in-depth by SEM, HRTEM, *in situ* XRD, XPS, Raman spectroscopy, and CO-DRIFTS.

Electron microscopy. The SEM images of Figure 2 show the microstructure of combustion-synthesized CeO_2 (one sample) and Ir-CeO_2 (two samples). There is no visible difference between Ir-free and Ir-loaded samples. The sponge-like structure is characteristic of ceria-based materials synthesized by combustion using such fuels as urea,[40] glycine,[41] or glycine-citric acid mixtures.[42] The round macropores are due to the fast evolution of gases during the highly exothermic combustion. Note that the texture of ceria prepared by other methods,[1] or even by SCS using ODH fuel (to be published), is completely different.

At the nanoscale, the material exhibits a hollowed puzzle-like structure, as shown by the HRTEM images of Figure 3 (see a-b and e-f). As a matter of fact, flat single-crystalline ceria sheets (see in particular the inset of Fig. 3b), fixed to each other by grain boundaries, are observed. However, holes are often present between the grains. The superimposition of the ceria sheets generates Moiré patterns in the TEM images (see Fig. 3b and inset, and Fig. 3c-e). This layered structure is consistent with the presence, in the N_2 adsorption/desorption isotherms, of an hysteresis of type H3, which corresponds to aggregates of plate-like particles giving rise to slit-shaped pores.[43]

Moreover, the grain edges or surfaces show a rough structure in the as-prepared samples (Fig. 3a). This amorphous structure is ascribed to residual carbonaceous deposits. Unlike for pure CeO_2, the presence of organic residues following the combustion synthesis of Ir-CeO_2 was evidenced by thermogravimetry coupled to mass spectrometry (Fig. S6). After the aforementioned treatments (reduction or oxidation-reduction) or the catalytic tests, the ceria grain surface appears much flatter (Fig. 3b-d), with clean (111) and (110) facets (Fig. 3c).

As far as iridium is concerned, both as-prepared and treated samples exhibit nanoparticles of 1.7 ± 0.9 nm in size (defined as the diameter of the circle with same surface area as the particle image). However, the number of nanoparticles is superior in the treated materials (compare Fig. 3a and Fig. 3b for 0.93 wt% Ir-CeO_2). This suggests that, as expected from one-step SCS, in the as-prepared samples part of iridium would be atomically dispersed in cationic form in the ceria matrix or present as small oxidic clusters on the ceria surface, and would coexist with IrO_x nanoparticles (see below). The thermal treatments would lead to extraction of the Ir ions from ceria and/or coalescence of small clusters, generating additional nanoparticles. In the case of SCS catalysts, the severe thermal treatments (at up to 900 °C in N_2 flow) do not induce any Ir particle size change. For example, for 0.11 wt% Ir-CeO_2, the Ir particle size after annealing at 900 °C and SRM is 1.8 ± 0.5 nm. The high-resolution images of Figure 3d show face-centered-cubic Ir nanoparticles (1.5-2.0 nm) exposing (111)

and (100) facets. The impregnation of SCS-CeO_2 with Ir salt and the subsequent heating in H_2 leads to Ir nanoparticles with similar sizes and shapes as those generated from one-step SCS, with low-index surface facets in both cases (Fig. 3e). After SRM tests, the impregnated Ir/CeO_2 exhibits a slight increase of the mean particle size (from 1.3 to 1.6 nm), which, together with its stronger affinity to carbon, may explain its inferior performances.[37]

CO-DRIFTS. In order to clarify the oxidic or metallic nature of the active Ir phase observed by TEM, and the effect of the standard reducing pretreatment (400 °C, H_2 flow) on this phase, as-prepared and reduced SCS materials were characterized by CO-DRIFTS at 50 °C under He flow, after exposure to a 1 % CO + He flow. The results are presented in Figure 4. Bare ceria, whether fresh or reduced, does not show any indication of CO adsorption in linear form.[44,45] The fresh Ir-CeO_2 sample adsorbs CO in small amount. Conversely, after catalyst heating in H_2, a strong infrared absorption band centered at 2046 cm^{-1} and due to C-O stretching vibration corresponding to linear ("on-top") adsorption of CO on metallic Ir (Ir-monocarbonyls), is visible.[46,47] Put together, these results are consistent with the presence of an Ir oxide surface phase on the fresh sample.

The band shape is somewhat different from the one recorded by DRIFTS at 100 °C in CO flow by Huang *et al.* on reduced 2 wt% Ir/CeO_2 catalysts prepared by deposition-precipitation or co-precipitation.[48] In these cases, a band centered at 2050 cm^{-1} with a shoulder at 2063 cm^{-1}, attributed to CO species linearly adsorbed on different Ir^0 sites, was observed. Even more different is the band shape observed at RT, after CO exposure and evacuation, by Nylén *et al.* on reduced 2 wt% Ir/20 wt% Al_2O_3-CeO_2 catalysts prepared by IWI.[49] The FTIR spectra exhibited a strong peak at 2075 cm^{-1} with a shoulder at 2003 cm^{-1}, both ascribed to Ir-dicarbonyl species.

Examining the apparently contradictory results of the literature pointed out by Nylén *et al.*,[49] the IR feature of Figure 4 suggests that our reduced Ir-CeO_2 sample is constituted of homogeneous Ir nanoparticles, giving rise to on-top (2046 cm^{-1} peak) and bridge-bonded (low-frequency tail) CO adsorption. The absence of Ir-dicarbonyls in the DRIFT spectrum rules out the presence of isolated Ir atoms or small clusters at the ceria surface.[49]

XRD. In addition to standard XRD analyses, *in situ* XRD experiments, in which the samples were heated up to 750 °C in H_2 flow, were carried out. Figure 5a shows the diffractograms of CeO_2 and 0.93 wt% Ir-CeO_2 recorded at RT in H_2 at the beginning and the end of these experiments. The X-ray diffractograms of all the SCS-prepared materials exhibit the fluorite structure of standard CeO_2 (space

group Fm-3m, #225), as in the examples of Figure 5a. The insert shows that, for the 1 wt% Ir sample, a signal associated to iridium is visible (Ir(111) line), although the corresponding peaks are very small and broad due to the small size of the Ir nanoparticles. Moreover, there is no extensive change of this feature after the series of measurements at up to 750 °C in H_2, which confirms the high resistance of Ir-CeO_2 toward metal nanoparticle sintering. The slight increase of the peak area is most likely due to the full reduction of the original IrO_x phase.

The average size of the ceria grains throughout the entire as-prepared sample series was determined to be in the 14-54 nm range (Table 1). Figure 5b shows *in situ* XRD results corresponding to the coarsening of ceria grains during temperature annealing in H_2 atmosphere. The sizes were determined from Rietveld analysis of the data. The average grain size for pure ceria, which is initially 14 nm, starts increasing above 450 °C, and reaches 60 nm at 750 °C (the final BET surface area is 6.7 $m^2\ g^{-1}$, *vs.* 22 $m^2\ g^{-1}$ before treatment). Note that the grain size does not evolve below 450 °C, which confirms the relevance of our standard pretreatment at 400 °C. Besides, as previously reported for other noble metals,[50] the presence of Ir limits the support coarsening: the average grain size increases from 26 to only 36 nm when going from 450 to 750 °C. Additional measurements on samples heated to 900 °C in N_2 and submitted to SRM tests at 750 °C show the same trends: 60 nm for 0.11 wt% Ir-CeO_2 *vs.* 85 nm for CeO_2(A). The corresponding surface areas are *ca*. 6 and 7 m^2/g, respectively.

Table 1 shows the lattice parameter (*a*) values of the as-prepared samples, derived from Rietveld refinement of the diffractograms recorded in ambient air. It appears that *a* is strongly dependent on the Ir loading and the preparation procedure. While for CeO_2 and 0.11 wt% Ir-CeO_2, *a* is in the 5.4119-5.4130 Å range, it increases to 5.4147-5.4148 Å for 0.93 wt% Ir-CeO_2. As the Ir ionic radii (<0.68 Å) are smaller than the Ce ones (>0.87 Å),[51] the increase in lattice parameter cannot be due to Ir insertion into the ceria lattice. Instead, this lattice parameter change is ascribed to the presence of Ce^{3+}, the ionic radius of which is bigger than the Ce^{4+} one (0.97 Å *vs.* 1.14 Å for 8 coordination). The reduction of Ce^{4+} to Ce^{3+} is generally accompanied by the formation of oxygen vacancies (V_O) to compensate the net charge decrease, following the formal equation: $Ce_4(IV)O_8 \rightarrow Ce_2(IV)Ce_2(III)O_7 + V_O$. As a result, the relationship between Ce^{3+} and oxygen vacancy concentrations is: $[Ce^{3+}] \approx 4\ [V_O]$. The lattice parameter variation for 0.93 wt% Ir-CeO_2 with respect to CeO_2 is: $\Delta a/a < 0.055$ %. According to the measurements of Alayoglu *et al.* on CeO_2 and Pt/CeO_2, this corresponds to *ca.* 1% of oxygen vacancies.[52] In our case, the (moderate) reduction of ceria is ascribed to the strong interaction between Ir and CeO_2,[53] with the formation of such entities as Ir^{x+}-O^{2-}-Ce^{3+}, as will be shown below.

Revised manuscript submitted to *J. Mater. Chem. A*

The various thermo-chemical treatments (including catalytic SRM tests) at up to 900 °C have no significant effect on the lattice parameter when measured in air (not shown). However, the values determined in H_2 for the two samples after the *in situ* experiments of Figure 5 are 0.025 % greater than those measured just after return to ambient air, consistently with the *in situ* (moderate) reduction of ceria and its subsequent re-oxidation in air.

XPS. XPS analyses of ceria and iridium-ceria samples were carried out to determine the amounts and oxidation states of Ir and Ce species, and to examine the influence of the preparation method (SCS *vs.* IWI) and the thermo-chemical treatments (as-prepared *vs.* reduction). The Ir 4f spectra of as-prepared and reduced 0.93 wt% Ir-CeO_2 SCS samples are shown in Figure 6a, and the numerical fit results are reported in Table 2. At the surface of the fresh SCS sample, Ir is present in three oxidation states: 43 % Ir^0 (metallic Ir, the binding energy for the $4f^{7/2}$ peak is $60 \leq E < 61$ eV), 39 % Ir^{x+} (Ir_2O_x with $0 < x < 4$, $61 \leq E < 62$ eV), and 18 % Ir^{4+} (IrO_2, $62 \leq E \leq 63$ eV).[54–57] The *in situ* reductive treatment at 400 °C suppresses the Ir^{4+} component, and two contributions remain: 79 % Ir^0 and 21 % Ir^{x+}. The latter is most likely related to Ir ions in contact with the support.[57] The extent of Ir oxidation depends on the sample preparation method and treatment. Whatever the treatment, the oxidation extent is superior in the SCS samples. In the case of the reduced catalysts, this suggests a stronger interaction of Ir with ceria for the SCS material. Moreover, the difference in Ir oxidation within the fresh IWI sample with respect to the reduced one shows that *ca.* 30 % of Ir was oxidized in air. This is noticeable since the IWI method ends with a reductive treatment in order to decompose the precursor salt.

Figure 6b shows the Ce 3d core-level results for CeO_2 and 0.93 wt% Ir-CeO_2 SCS samples. For the sake of comparison, the CeO_2 sample was also sputtered *in situ* with Ar^+ ions in order to reduce it to near-Ce_2O_3 surface stoichiometry (as indicated by the quasi disappearance of the u''' peak, see Fig. 6b).[58,59] The spectra of fresh Ir-CeO_2 SCS sample (Fig. 6b), and fresh or reduced Ir/CeO_2 IWI samples (Fig. S7), are nearly identical to that of pre-calcined CeO_2 (Fig. 6b), suggesting a very limited extent of Ir-induced surface reduction in these cases. As a matter of fact, the $Ce^{3+}/(Ce^{3+}+Ce^{4+})$ fraction is lower than 3%. Only the Ir-CeO_2 (SCS) sample heated in H_2 at 400 °C exhibits a difference. In particular, one can observe a slightly more intense signal around 885 eV (v' contribution, Fig. 6b), which suggests an increased amount of Ce^{3+} species.[58,60] Indeed, fitting the Ce spectrum with a linear combination of CeO_2 (pre-calcined sample) and Ce_2O_3 (sputtered sample) reference spectra,[61] we estimate the Ce^{3+} concentration to 7% (Fig. S7). This amount is significant for such a low temperature of reducing

treatment,[62] and is consistent with a stronger Ir-ceria interaction giving rise to enhanced catalytic performances for the SCS materials as compared to the IWI ones.

µRaman spectroscopy. The Raman spectra of CeO_2 and 0.93 wt% Ir-CeO_2 as-prepared SCS samples are plotted between 200 and 1800 cm^{-1} in Figure 7a. They exhibit an intense band attributed to triply degenerate F_{2g} mode of CeO_2 with fluorite structure (space group O_h^5), which can be viewed as a symmetric breathing mode of the oxygen anions around Ce cations.[63–66] This peak is centered at 461 cm^{-1} for the noble metal-containing sample, versus 466 cm^{-1} for pristine CeO_2. This significant red-shift is attributed to weaker force constants of Ce-O bonds associated with a larger lattice parameter (5.4147 *vs.* 5.4123 Å, see Table 1). In fact, a continuous red-shift of the F_{2g} mode with the Ir content is observed in Figure 7b. Furthermore, a linear correlation between the peak full width at half-maximum and its position is clearly established: the higher the red-shift, the broader the band. The broadening could arise from higher phonon confinement in CeO_2 nanoparticles,[63,65,67] but this hypothesis is ruled out since the crystallite size determined from XRD analysis does not vary significantly with the Ir content (Table 1). Therefore, the broadening is ascribed to the presence of Ce^{3+} cations and oxygen vacancies within the CeO_2 lattice, which induce disorder and decrease the bond strength.[68–70]

Figure 7c displays a zoom around the bottom of the main Raman peak (300-1000 cm^{-1} range) for the series of spectra recorded on fresh and reduced samples with various Ir loadings. It reveals a weak band at 575 cm^{-1} and a shoulder around 670 cm^{-1}. Noticeably, these features do not correspond to those observed for IrO_2 (tetragonal rutile), since the Raman main bands of this oxide are located around 555, 720 and 740 cm^{-1}.[71,72] The band at 575 cm^{-1} could originate in part from a stretching vibration mode involving oxygen vacancies.[65,66] Indeed, it is extensively reported in the literature that the relative intensity of this band increases with the divalent or trivalent dopant content in the bulk.[69,70,73–75] Consistently, here the relative intensity of the band at 575 cm^{-1} increases with the Ir content, confirming that the presence of Ir favors the formation of oxygen vacancies and Ce^{3+} cations. Murell *et al.* have observed broad bands at 622 and 614 cm^{-1} for 2.4 wt% and 4.9 wt% Ir/CeO_2-Al_2O_3 catalysts, respectively, and assigned them to Ir-O surface structures.[76,77] Therefore, the band at 575 cm^{-1} could be composed of two sub-features arising from oxygen vacancies (around 560 cm^{-1}) and IrO_x particles (around 600 cm^{-1}). Consistently, for 0.93 wt% Ir-CeO_2 (Fig. 7c), this band is shifted from 575 to *ca.* 560 cm^{-1}, and slightly enhanced after reduction, due to the formation of oxygen vacancies and the disappearance of the IrO_x phase. The same trend is observed for 0.11 wt%

Ir-CeO_2 upon reduction (Fig. 7c). Finally, the shoulder around 670 cm^{-1}, observed even for low metal loadings, is ascribed to Ir-O-Ce stretching vibrations at the surface of CeO_2 crystallites.

Conclusions

Iridium (0.06-0.93 wt%)-loaded oxide nanopowders were synthesized for the first time by a combustion method, namely solution combustion synthesis. The ceria-based materials exhibited the fluorite structure with a crystallite size of *ca*. 30 nm (XRD) and a specific surface area of *ca*. 20 $m^2\ g^{-1}$ (BET). They are mesoporous with a unique sponge-like texture, as observed by SEM. Aberration-corrected HRTEM allowed us to image the peculiar structure and arrangement of ceria crystallites, which are made of superimposed flat layers, and assemble themselves like in an incomplete puzzle. Upon reduction in H_2, faceted Ir nanoparticles of 1-3 nm in size are present at the ceria surface, and their morphology and size appear unaffected by thermochemical treatments at up to 900 °C.

In situ XRD experiments showed that the iridium-ceria materials are resistant to ceria grain sintering (*e.g.*, crystallite size 37 nm for 1 wt% Ir-CeO_2 *vs.* 60 nm for CeO_2 at 750 °C in H_2). In the as-prepared samples, iridium is present both in metallic (XPS, XRD) and oxidic (XPS, Raman) forms. The quasi absence of CO adsorption on these samples, as attested by CO-DRIFTS, suggests that the nanoparticles observed by TEM on as-prepared 0.93 wt% Ir-CeO_2 are oxidized at their surface. The oxide layer is in the IrO_x form, with at least two oxidation states: x ($0 < x \leq 4$) and IV. On the samples treated in hydrogen, a significant fraction (20 % for 0.93 wt% Ir-CeO_2) of Ir^{x+} species remains, most probably at the iridium-ceria interface.

The oxidation state of ceria and the presence of oxygen vacancies were investigated by combining XPS, XRD and Raman data. The addition of Ir to ceria leads to an increase of the lattice parameter, correlated with the formation of a small amount of oxygen vacancies and Ce^{3+} cations (up to 7 % Ce^{3+} in reduced 0.93 wt% Ir-CeO_2). The latter are present within Ir^{x+}-O^{2-}-Ce^{3+} species at the surface of ceria crystallites. No signs of Ir ion insertion into the ceria lattice were evidenced.

The materials were used as catalysts in the production of hydrogen from the steam reforming of methane in water-deficient conditions (CH_4/H_2O molar ratio = 10) at 700-750 °C, *i.e.*, highly severe conditions, such as those present in methane-fueled SOFCs. The catalysts appeared more active and stable than catalysts prepared by conventional incipient wetness impregnation. The superior activity of the SCS catalysts correlates with their higher reactivity with methane and lower reactivity with carbon, as evidenced by temperature-programmed experiments. The better performances of Ir-CeO_2 are ascribed to the slightly higher Ir dispersion (HRTEM) and stronger metal-oxide interaction (XPS)

provided by solution combustion synthesis. This method appears as a simple and cost-effective way of synthesizing in one step ceria-based catalysts doped with small amounts of noble metals for high-temperature catalysis devoted to sustainable energy production.

Acknowledgement

TSN, FM, and LP acknowledge the French National Research Agency for funding through the ANR-BS10-009 "DINAMIC" project. GP thanks the CNRS for financial support accompanying her Chaire d'Excellence position. Y. Aizac (XRD), N. Cristin & P. Mascunan (ICP, BET), and L. Cardenas (XPS) are greatly thanked for technical support and discussions. E. Pouliquen is acknowledged for her participation to synthesis and catalysis experiments. Thanks are due to the CLYM and T. Epicier for access to the FEI Titan microscope (CLYM is supported by the CNRS, the "Grand Lyon" and the Rhône-Alpes Region). LP acknowledges the European COST Action CM1104 "Red ox" for stimulating networking discussions.

References

1. A. Trovarelli and P. Fornasiero, *Catalysis by Ceria and Related Materials: 2nd Edition*, Imperial College Press, 2013.
2. J. Paier, C. Penschke, and J. Sauer, *Chem. Rev.*, 2013, **113**, 3949–3985.
3. C. T. Campbell, *Science*, 2005, **309**, 713–714.
4. L. Vivier and D. Duprez, *ChemSusChem*, 2010, **3**, 654–678.
5. M. Mogensen, N. M. Sammes, and G. A. Tompsett, *Solid State Ionics*, 2000, **129**, 63–94.
6. B. Shri Prakash, S. Senthil Kumar, and S. T. Aruna, *Renewable Sustainable Energy Rev.*, 2014, **36**, 149–179.
7. E. P. Murray, T. Tsai, and S. A. Barnett, *Nature*, 1999, **400**, 649–651.
8. P. Vernoux, J. Guindet, and M. Kleitz, *J. Electrochem. Soc.*, 1998, **145**, 3487–3492.
9. W. Cai, F. Wang, E. Zhan, A. C. Van Veen, C. Mirodatos, and W. Shen, *J. Catal.*, 2008, **257**, 96–107.
10. F. Wang, W. Cai, H. Provendier, Y. Schuurman, C. Descorme, C. Mirodatos, and W. Shen, *International Journal of Hydrogen Energy*, 2011, **36**, 13566–13574.
11. W. Cai, F. Wang, C. Daniel, A. C. van Veen, Y. Schuurman, C. Descorme, H. Provendier, W. Shen, and C. Mirodatos, *J. Catal.*, 2012, **286**, 137–152.
12. J. Toyir, P. Gélin, H. Belatel, and A. Kaddouri, *Catal. Today*, 2010, **157**, 451–455.
13. G. Postole, K. Girona, J. Toyir, A. Kaddouri, and P. Gélin, *Fuel Cells*, 2012, **12**, 275–287.
14. S. L. González-Cortés and F. E. Imbert, *Appl. Catal. A*, 2013, **452**, 117–131.
15. W. Shan, Z. Feng, Z. Li, J. Zhang, W. Shen, and C. Li, *J .Catal.*, 2004, **228**, 206–217.
16. J. Papavasiliou, G. Avgouropoulos, and T. Ioannides, *Appl. Catal. B*, 2006, **66**, 168–174.
17. P. Yaseneva, S. Pavlova, V. Sadykov, E. Moroz, E. Burgina, L. Dovlitova, V. Rogov, S. Badmaev, S. Belochapkin, and J. Ross, *Catal. Today*, 2008, **138**, 175–182.
18. V. M. Gonzalez-Delacruz, F. Ternero, R. Pereniguez, A. Caballero, and J. P. Holgado, *Appl. Catal. A*, 2010, **384**, 1–9.

19. L. Pino, A. Vita, F. Cipiti, M. Lagana, and V. Recupero, *Appl. Catal. B*, 2011, **104**, 64–73.
20. D. H. Prasad, S. Y. Park, H. Ji, H.-R. Kim, J.-W. Son, B.-K. Kim, H.-W. Lee, and J.-H. Lee, *Appl. Catal. A*, 2012, **411**, 160–169.
21. M. S. Hegde, G. Madras, and K. C. Patil, *Acc. Chem. Res.*, 2009, **42**, 704–712.
22. P. Bera and M. Hegde, *Catal. Surv. Asia*, 2011, **15**, 181–199.
23. P. Bera, K. R. Priolkar, P. R. Sarode, M. S. Hegde, S. Emura, R. Kumashiro, and N. P. Lalla, *Chem. Mater.*, 2002, **14**, 3591–3601.
24. K. R. Priolkar, P. Bera, P. R. Sarode, M. S. Hegde, S. Emura, R. Kumashiro, and N. P. Lalla, *Chem. Mater.*, 2002, **14**, 2120–2128.
25. P. Bera, K. R. Priolkar, A. Gayen, P. R. Sarode, M. S. Hegde, S. Emura, R. Kumashiro, V. Jayaram, and G. N. Subbanna, *Chem. Mater.*, 2003, **15**, 2049–2060.
26. A. Gayen, K. R. Priolkar, P. R. Sarode, V. Jayaram, M. S. Hegde, G. N. Subbanna, and S. Emura, *Chem. Mater.*, 2004, **16**, 2317–2328.
27. L. Pino, A. Vita, F. Cipiti, M. Lagana, and V. Recupero, *Appl. Catal. A*, 2006, **306**, 68–77.
28. N. Russo, D. Fino, G. Saracco, and V. Specchia, *Catal. Today*, 2006, **117**, 214–219.
29. S. Specchia, E. Finocchio, G. Busca, P. Palmisano, and V. Specchia, *J. Catal.*, 2009, **263**, 134–145.
30. U.-E.-S. Amjad, A. Vita, C. Galletti, L. Pino, and S. Specchia, *Ind. Eng. Chem. Res.*, 2013, **52**, 15428–15436.
31. S. Colussi, A. Gayen, M. Farnesi Camellone, M. Boaro, J. Llorca, S. Fabris, and A. Trovarelli, *Angew. Chem. Int. Ed.*, 2009, **48**, 8481–8484.
32. A. Gayen, M. Boaro, C. de Leitenburg, J. Llorca, and A. Trovarelli, *J. Catal.*, 2010, **270**, 285–298.
33. S. Colussi, A. Gayen, J. Llorca, C. de Leitenburg, G. Dolcetti, and A. Trovarelli, *Ind. Eng. Chem. Res.*, 2012, **51**, 7510–7517.
34. G. Avgouropoulos, J. Papavasiliou, and T. Ioannides, *Chem. Eng. J.*, 2009, **154**, 274–280.
35. V. M. Shinde and G. Madras, *Appl. Catal. B*, 2013, **132–133**, 28–38.
36. S. R. Jain, K. C. Adiga, and V. R. Pai Verneker, *Combust. Flame*, 1981, **40**, 71–79.
37. G. Postole, T. S. Nguyen, M. Aouine, P. Gélin, L. Cardenas, and L. Piccolo, *Appl. Catal. B*, 2014, **submitted**.
38. S.-S. Chang, B. Clair, J. Ruelle, J. Beauchene, F. Di Renzo, F. Quignard, G.-J. Zhao, H. Yamamoto, and J. Gril, *J. Exp. Bot.*, 2009, **60**, 3023–3030.
39. F. Mariño, C. Descorme, and D. Duprez, *Appl. Catal. B*, 2004, **54**, 59–66.
40. C.-C. Hwang, T.-H. Huang, J.-S. Tsai, C.-S. Lin, and C.-H. Peng, *Mater. Sci. Eng. B*, 2006, **132**, 229–238.
41. D. H. Prasad, H.-Y. Jung, H.-G. Jung, B.-K. Kim, H.-W. Lee, and J.-H. Lee, *Mater. Lett.*, 2008, **62**, 587–590.
42. H. Palneedi, V. Mangam, S. Das, and K. Das, *J. Alloys Compd.*, 2011, **509**, 9912–9918.
43. K. S. W. Sing, D. H. Everett, R. A. W. Haul, L. Moscou, R. A. Pierotti, J. Rouquérol, and T. Siemieniewska, *Pure Appl. Chem.*, 1985, **57**, 603–619.
44. C. Li, Y. Sakata, T. Arai, K. Domen, K. Maruya, and T. Onishi, *J. Chem. Soc., Faraday Trans. 1*, 1989, **85**, 929–943.
45. F. Bozon-Verduraz and A. Bensalem, *J. Chem. Soc., Faraday Trans.*, 1994, **90**, 653–657.
46. R. W. Boyle, J. Lauterbach, M. Schick, W. J. Mitchell, and W. H. Weinberg, *Ind. Eng. Chem. Res.*, 1996, **35**, 2986–2992.
47. A. Erdohelyi, K. Fodor, and G. Suru, *Appl. Catal. A*, 1996, **139**, 131–147.
48. Y. Huang, A. Wang, L. Li, X. Wang, D. Su, and T. Zhang, *J .Catal.*, 2008, **255**, 144–152.
49. U. Nylén, L. Sassu, S. Melis, S. Järås, and M. Boutonnet, *Appl. Catal. A*, 2006, **299**, 1–13.
50. S. Hosokawa, M. Taniguchi, K. Utani, H. Kanai, and S. Imamura, *Applied Catalysis A: General*, 2005, **289**, 115–120.
51. R. D. Shannon, *Acta Cryst. A*, 1976, **32**, 751–767.
52. S. Alayoglu, K. An, G. Melaet, S. Chen, F. Bernardi, L. W. Wang, A. E. Lindeman, N. Musselwhite, J. Guo, Z. Liu, M. A. Marcus, and G. A. Somorjai, *J. Phys. Chem. C*, 2013, **117**, 26608–26616.
53. J. A. Farmer and C. T. Campbell, *Science*, 2010, **329**, 933–936.
54. M. Peuckert, *Surf. Sci.*, 1984, **144**, 451–464.

55. S. Thanawala, D. G. Georgiev, R. J. Baird, and G. Auner, *Thin Solid Films*, 2007, **515**, 7059–7065.
56. W.-H. Chung, D.-S. Tsai, L.-J. Fan, Y.-W. Yang, and Y.-S. Huang, *Surf. Sci.*, 2012, **606**, 1965–1971.
57. S. Nassreddine, L. Massin, M. Aouine, C. Geantet, and L. Piccolo, *J. Catal.*, 2011, **278**, 253–265.
58. A. Pfau and K. D. Schierbaum, *Surf. Sci.*, 1994, **321**, 71–80.
59. J. P. Holgado, R. Alvarez, and G. Munuera, *Appl. Surf. Sci.*, 2000, **161**, 301–315.
60. E. Paparazzo, *Mater. Res. Bull.*, 2011, **46**, 323–326.
61. C. Zhang, M. E. Grass, A. H. McDaniel, S. C. DeCaluwe, F. E. Gabaly, Z. Liu, K. F. McCarty, R. L. Farrow, M. A. Linne, Z. Hussain, G. S. Jackson, H. Bluhm, and B. W. Eichhorn, *Nat. Mater.*, 2010, **9**, 944–949.
62. A. Laachir, V. Perrichon, A. Badri, J. Lamotte, E. Catherine, J. C. Lavalley, J. E. Fallah, L. Hilaire, F. L. Normand, E. Quéméré, G. N. Sauvion, and O. Touret, *J. Chem. Soc., Faraday Trans.*, 1991, **87**, 1601–1609.
63. W. H. Weber, K. C. Hass, and J. R. McBride, *Phys. Rev. B*, 1993, **48**, 178–185.
64. A. Nakajima, A. Yoshihara, and M. Ishigame, *Phys. Rev. B*, 1994, **50**, 13297–13307.
65. J. E. Spanier, R. D. Robinson, F. Zhang, S.-W. Chan, and I. P. Herman, *Phys. Rev. B*, 2001, **64**, 245407.
66. M. Daniel and S. Loridant, *J. Raman Spectrosc.*, 2012, **43**, 1312–1319.
67. I. Kosacki, T. Suzuki, H. U. Anderson, and P. Colomban, *Solid State Ionics*, 2002, **149**, 99–105.
68. Z. D. Dohčević-Mitrović, M. J. Šćepanović, M. U. Grujić-Brojčin, Z. V. Popović, S. B. Bošković, B. M. Matović, M. V. Zinkevich, and F. Aldinger, *Solid State Commun.*, 2006, **137**, 387–390.
69. G. Gouadec and P. Colomban, *Prog. Cryst. Growth Charact. Mater.*, 2007, **53**, 1–56.
70. V. Grover, A. Banerji, P. Sengupta, and A. K. Tyagi, *J. Solid State Chem.*, 2008, **181**, 1930–1935.
71. A. V. Korotcov, Y.-S. Huang, K.-K. Tiong, and D.-S. Tsai, *J. Raman Spectrosc.*, 2007, **38**, 737–749.
72. Y. M. Chen, Y. S. Huang, K. Y. Lee, D. S. Tsai, and K. K. Tiong, *J. Mater. Sci.: Mater. Electron.*, 2011, **22**, 890–894.
73. M.-F. Luo, Z.-L. Yan, L.-Y. Jin, and M. He, *J. Phys. Chem. B*, 2006, **110**, 13068–13071.
74. M. Guo, J. Lu, Y. Wu, Y. Wang, and M. Luo, *Langmuir*, 2011, **27**, 3872–3877.
75. L. G. Teoh and G. W. Chiang, *J. Sol-Gel Sci. Technol.*, 2012, **64**, 530–533.
76. L. L. Murrell, S. J. Tauster, and D. R. Anderson, *Stud. Surf. Sci. Catal.*, 1991, **71**, 275–289.
77. L. L. Murrell, S. J. Tauster, and D. R. Anderson, *Stud. Surf. Sci. Catal.*, 1993, **75**, 681–690.

Revised manuscript submitted to *J. Mater. Chem. A*

Table 1. Characteristics of the as-prepared samples.

Material	***Metal content (wt%)[a]***	***Mean ceria crystallite size / lattice parameter (nm)[b]***	***Specific surface area (m^2/g)[c]***
CeO_2 (A)	0	50 / 0.54123	22
CeO_2 (B)	0	40 / 0.54130	22
CeO_2 (C)	0	24 / 0.54134	28
CeO_2 (D)	0	14 / 0.54134	56
CeO_2 (E)	0	~35	-
CeO_2 (F)	0	~35	-
CeO_2 (G)	0	~31	-
CeO_2 (H) commercial	0	165 / 0.54121	4
Ir/CeO_2 (A) IWI acac[d]	0.14	31 / 0.54161	16
Ir/CeO_2 (B) IWI Cl[d]	0.33	~35	16
Ir/CeO_2 (C) IWI Cl[d]	0.56	~50	13
Ir-CeO_2 (A)	0.065	~35	16
Ir-CeO_2 (B)	0.090	~54	10
Ir-CeO_2 (C)	0.11	38 / 0.54124	~15
Ir-CeO_2 (D)	0.14	~52	11
Ir-CeO_2 (E)	0.18	~29	18
Ir-CeO_2 (F)	0.34	~26	-
Ir-CeO_2 (G)	0.93	26 / 0.54147	29

[a] Determined by ICP-OES; [b] Determined by XRD Rietveld refinements or Scherrer method (symbol ~); [c] Determined by N_2 adsorption volumetry (BET); [d] acac and Cl denote acetylacetonate and chloride Ir precursors, respectively. For the IWI samples, the as-prepared form corresponds to a reduced state.

Revised manuscript submitted to *J. Mater. Chem. A*

Table 2. Results of XPS analyses (Ir 4f core levels) of 0.93 wt% Ir-CeO_2 prepared by SCS and 0.56 wt% Ir/CeO_2 prepared by SCS+IWI, fresh or after *in situ* reducing (H_2, 400 °C) treatment.

Sample	***E*** *eV*	***ΔE*** *eV*	***A*** *%*	***E'*** *eV*	***ΔE'*** *eV*	***A'*** *%*	***E"*** *eV*	***ΔE"*** *eV*	***A"*** *%*
IWI reduced	59.9	1.16	84.0	61.1	1.25	16.0	-	-	-
IWI fresh	60.9	1.07	54.7	61.9	1.10	24.8	63.2	1.78	20.5
SCS reduced	59.9	1.35	79.4	61.3	1.46	20.5	-	-	-
SCS fresh	60.0	1.02	43.4	61.0	1.17	38.6	62.1	1.65	18.0
Attrib.	Ir^0			Ir^{x+}			Ir^{4+}		

For each contribution, *E*, *ΔE* and *A* correspond to the position, FWHM and relative area, respectively, obtained from numerical fitting of the Ir $4f^{7/2}$ peak.

Revised manuscript submitted to *J. Mater. Chem. A*

Figure 1. (a) Compared performances of CeO_2 (sample A, SCS), 0.11 wt% Ir-CeO_2 (SCS, "oxred") and 0.33 wt% Ir/CeO_2 (SCS+IWI) in steam reforming of methane to hydrogen. The inset shows the product distribution after 15 h on stream. Conditions: 750 °C, CH_4:H_2O:N_2 = 50:5:45, 1 atm, flow reactor. (b) H_2 and CO desorption rates during CH_4-TPR of the fresh catalysts.

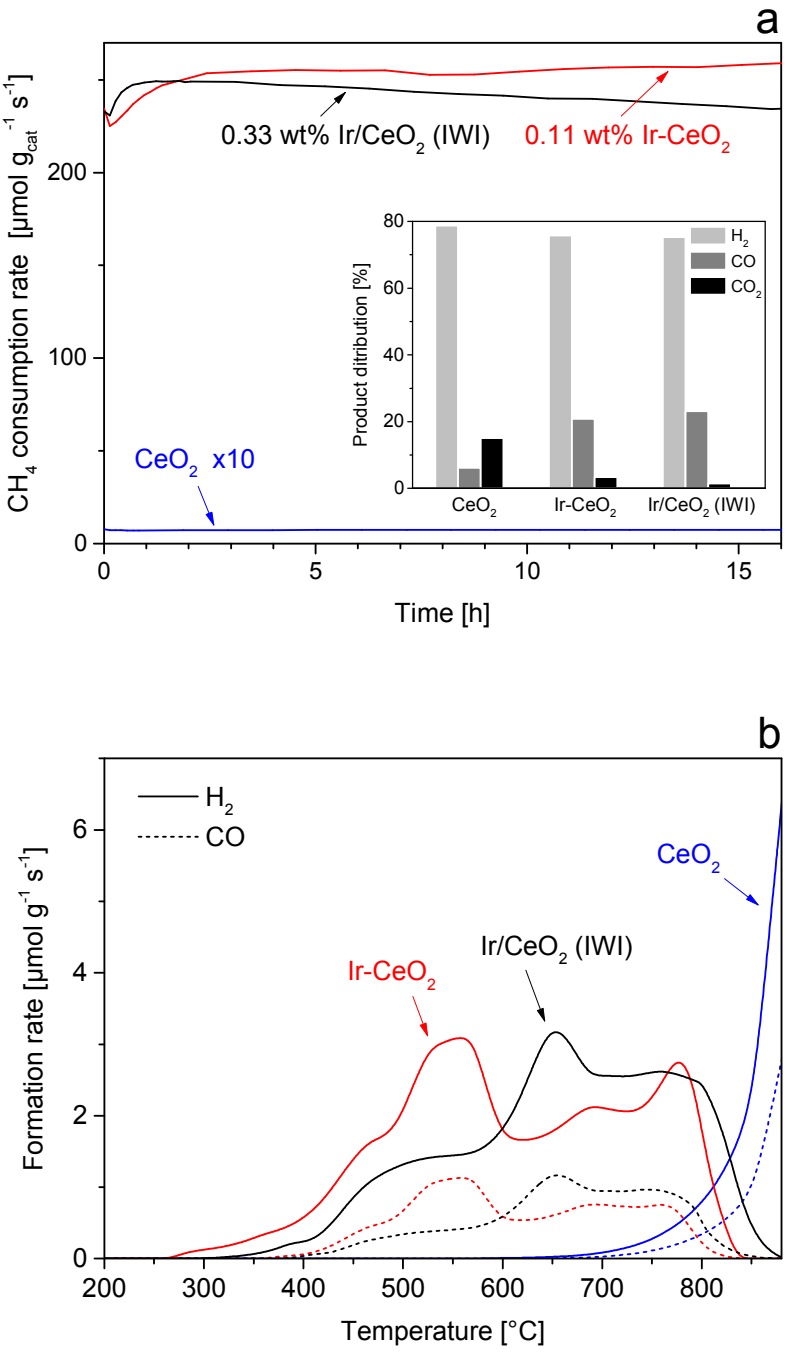

Revised manuscript submitted to *J. Mater. Chem. A*

Figure 2. SEM images of CeO_2(A) (a), 0.11 wt% Ir-CeO_2 (b and d), and 0.93 wt% Ir-CeO_2 (c) (as-prepared samples).

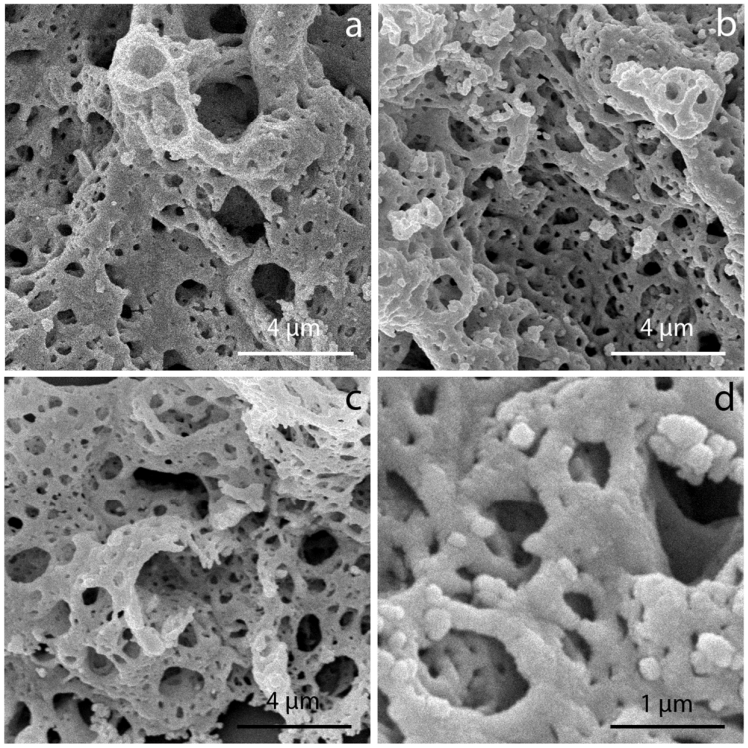

Revised manuscript submitted to *J. Mater. Chem. A*

Figure 3. Aberration-corrected TEM images of Ir-CeO_2 catalysts. (a) 0.93 wt% Ir-CeO_2 as-prepared; (b) 0.93 wt% Ir-CeO_2 reduced; (c) 0.11 wt% Ir-CeO_2 oxidized-reduced; (d) 0.11 wt% Ir-CeO_2 after SRM reaction; (e) 0.14 wt% Ir/CeO_2 (IWI) as-prepared; (f) 0.14 wt% Ir/CeO_2 (IWI) after SRM reaction.

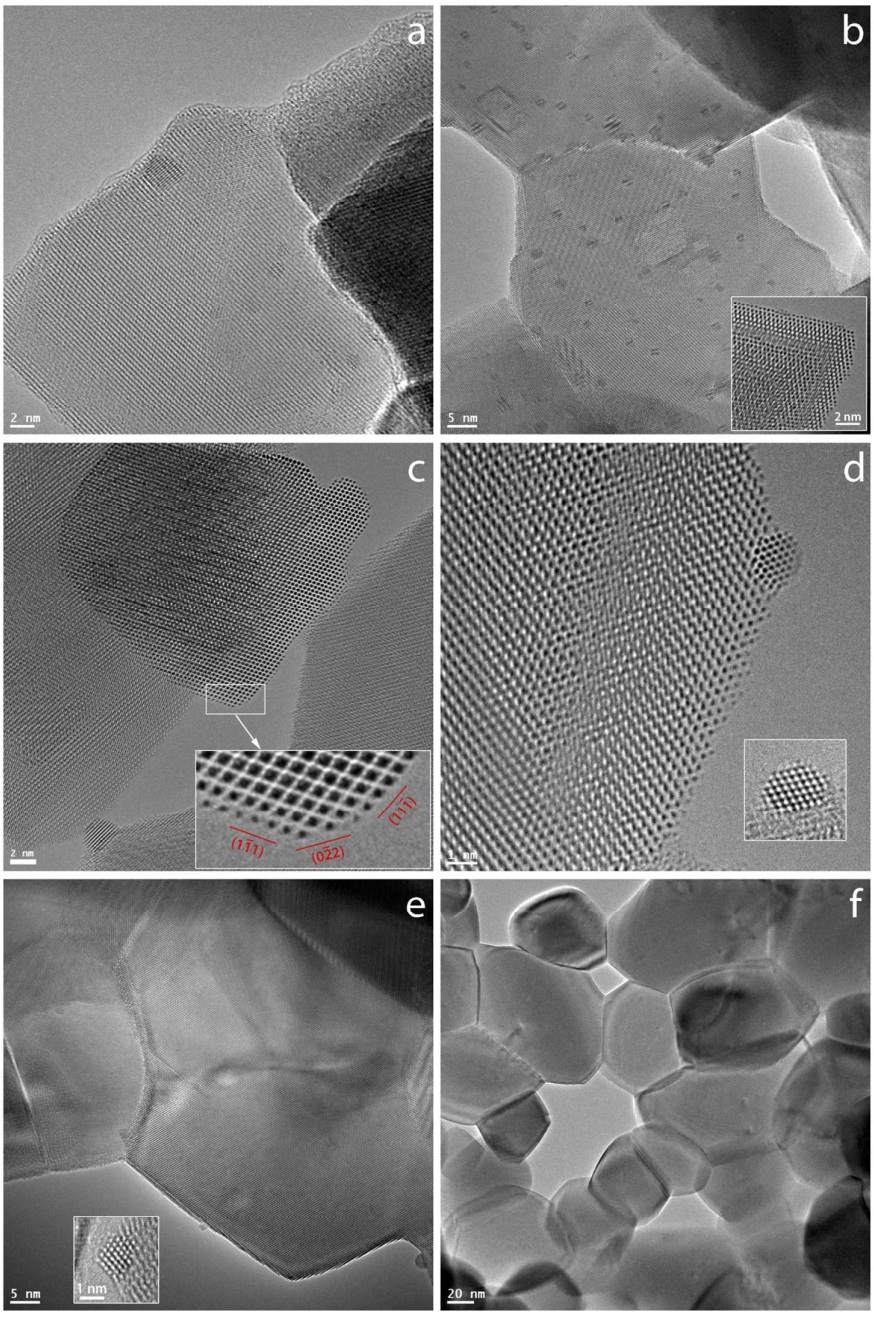

Revised manuscript submitted to *J. Mater. Chem. A*

Figure 4. DRIFTS spectra of pre-adsorbed CO measured at 50 °C on as-prepared and *in situ* reduced (H_2, 400 °C) CeO_2(A) and 0.93 wt% Ir-CeO_2 SCS samples.

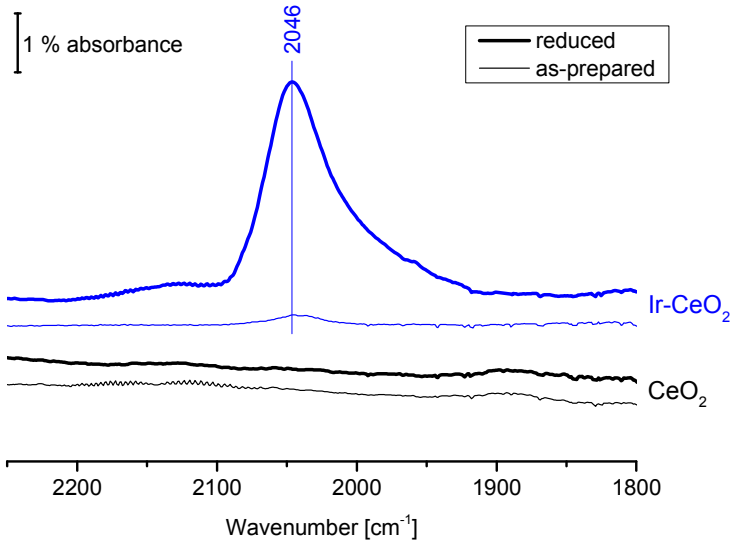

Revised manuscript submitted to *J. Mater. Chem. A*

Figure 5. (a) X-ray diffractograms for CeO_2(D) and 0.93 wt% Ir-CeO_2 samples recorded at 25 °C in H_2 atmosphere, before and after heating up to 750 °C. The inset shows a close view of the Ir(111) region of the diffractograms. (b) Evolution of ceria average crystal size with temperature in H_2 flow during *in situ* XRD experiments on the same samples as in (a).

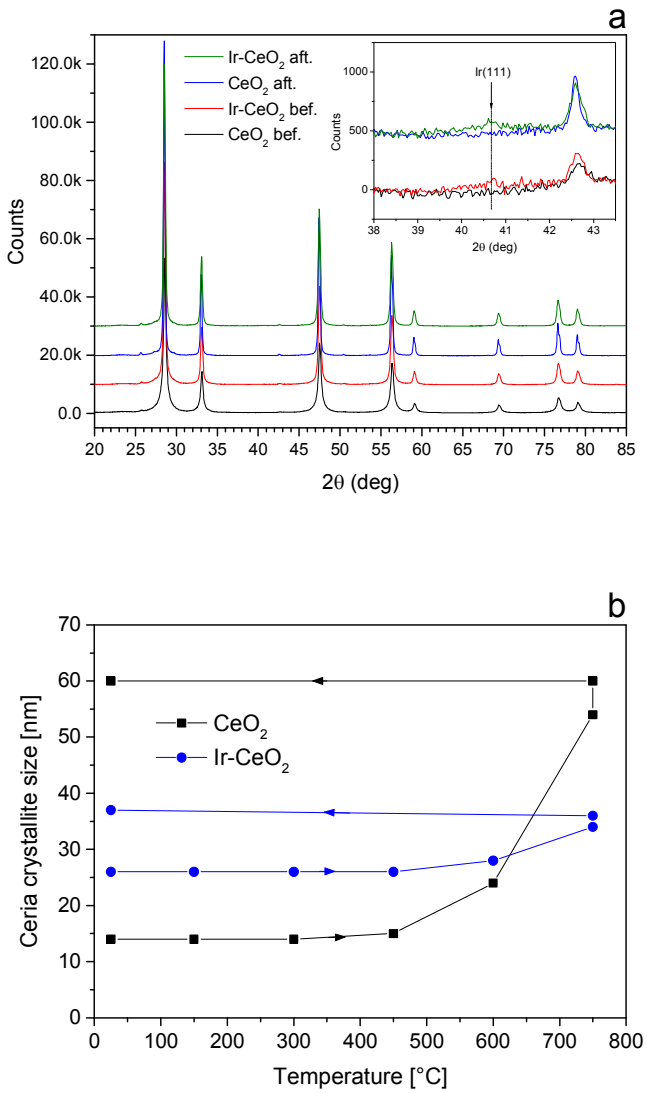

Revised manuscript submitted to *J. Mater. Chem. A*

Figure 6. XPS spectra: (a) Ir 4f core levels for as-prepared and *in situ* reduced (H_2, 400 °C) 0.93 wt% Ir-CeO_2 samples, along with numerical fits; (b) Ce 3d core levels for Ce_2O_3 (see text), calcined (air, 400 °C) CeO_2(A), and *in situ* reduced (H_2, 400 °C) 0.93 wt% Ir-CeO_2 samples.

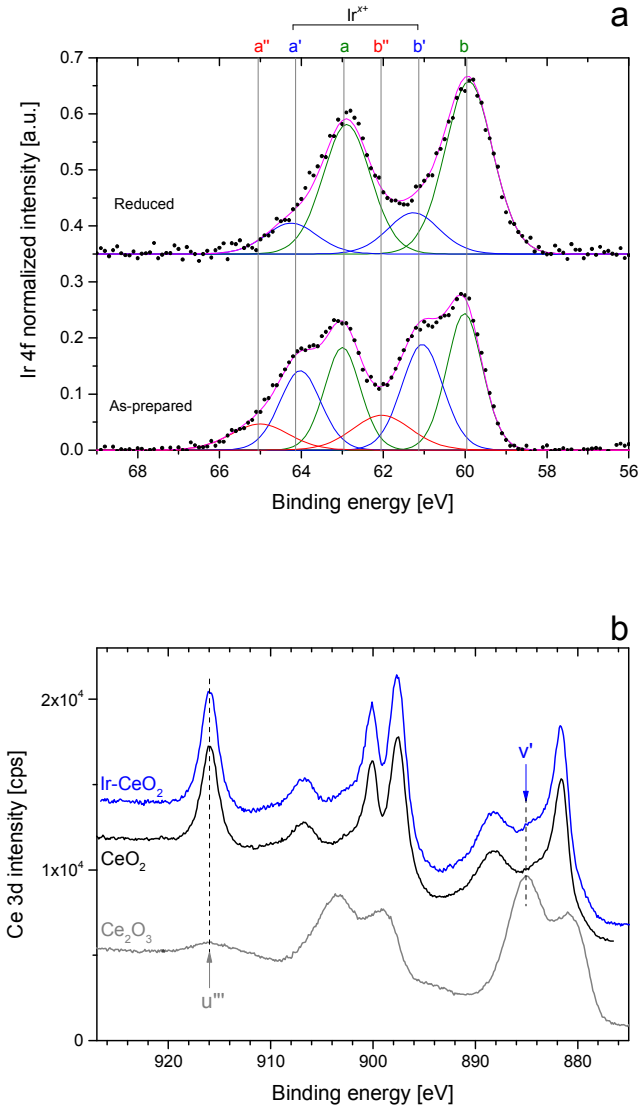

Revised manuscript submitted to *J. Mater. Chem. A*

Figure 7. (a) Raman spectra for as-prepared CeO_2(A) and 0.93 wt% Ir-CeO_2. The Y axis represents relative intensities in arbitrary units. (b) Full width at half-maximum versus position of the main Raman peak for as-prepared and *ex situ* reduced samples. (c) Corresponding Raman spectra. The assignments of the main contributions are schematized on the graph.

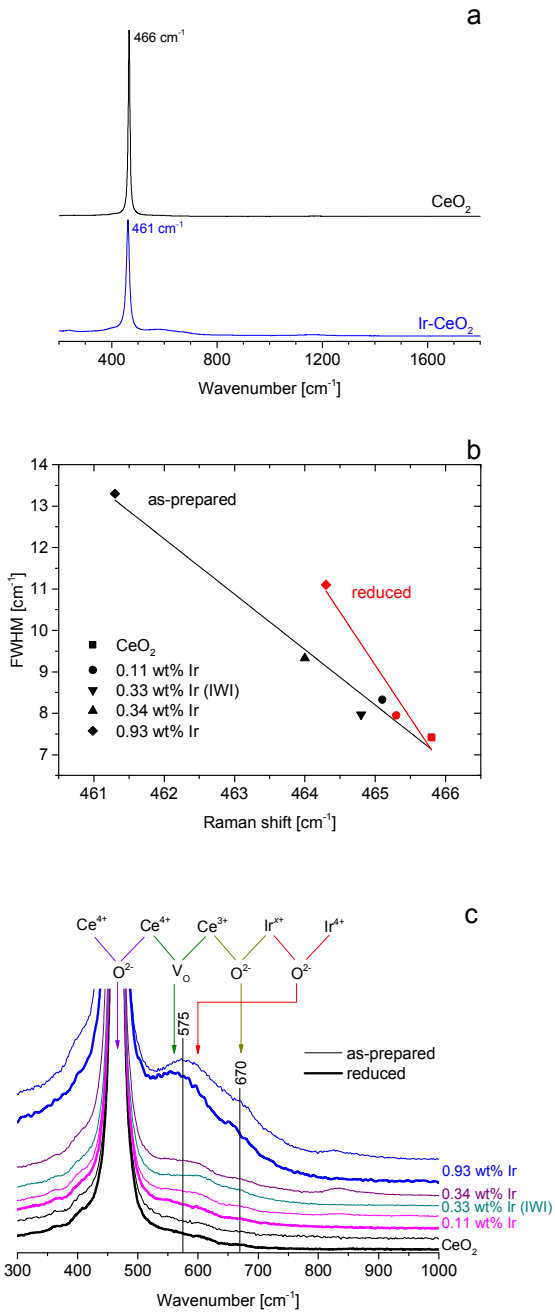

Ultrastable iridium-ceria nanopowders synthesized in one step by solution combustion for catalytic hydrogen production by T.S. Nguyen *et al*.

Graphical and textual abstract

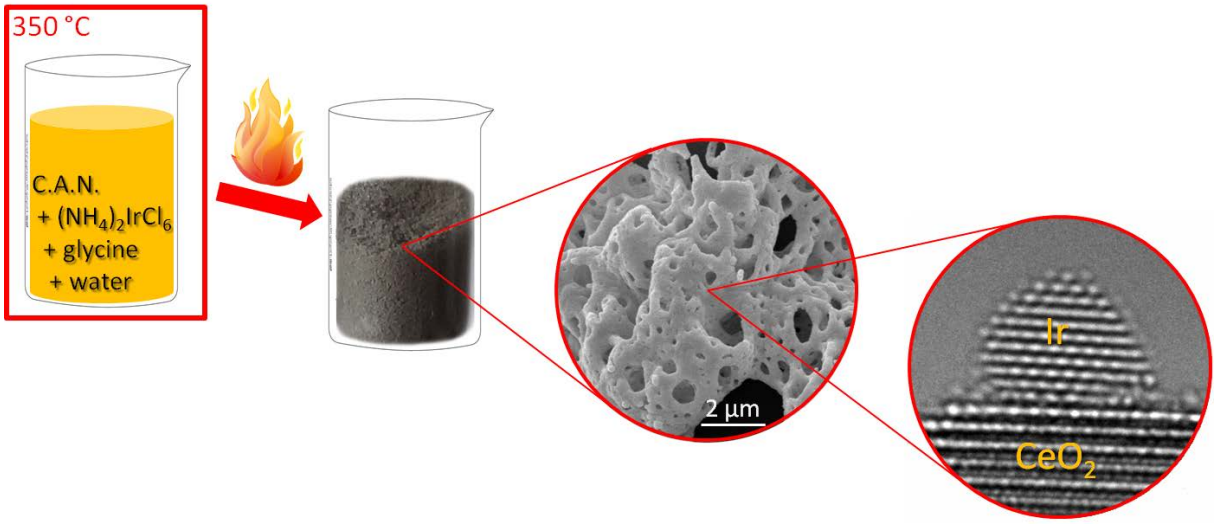

Ir nanoparticles strongly anchored on mesoporous ceria were synthesized in one step by solution combustion. This catalytic material is active and stable in the production of hydrogen from methane at high temperature.